

UCLA

UCLA Electronic Theses and Dissertations

Title

Origins of Reactivity and Selectivity of a Series of Proximity-Induced Transannular Diels-Alder Reactions

Permalink

<https://escholarship.org/uc/item/4g93x5sn>

Author

He, Cyndi Qixin

Publication Date

2013

Peer reviewed|Thesis/dissertation

UNIVERSITY OF CALIFORNIA

Los Angeles

Origins of Reactivity and Selectivity of a Series of Proximity-Induced Transannular Diels-Alder
Reactions

A thesis submitted in partial satisfaction of the requirements for the degree of Master of Science
in Chemistry

by

Qixin He

2013

ABSTRACT OF THE THESIS

Origins of Reactivity and Selectivity
of a Series of Proximity-Induced Transannular Diels-Alder Reactions

by

Qixin He

Master of Science in Chemistry

University of California, Los Angeles, 2013

Professor Kendall N. Houk, Chair

Transannular Diels-Alder (TADA) reactions are a powerful tool for the construction of polycyclic structures with four stereogenic centers. A series of remarkably facile and stereoselective TADA reactions was observed experimentally by Merlic and coworkers. In this thesis, the mechanism was modeled quantum mechanically and the controlling factors of the high stereoselectivity and reactivity of TADA were determined for these reactions and the analogous bimolecular and intramolecular Diels-Alder reactions.

The thesis of Qixin He is approved.

Craig A. Merlic

Neil K. Garg

Kendall N. Houk, Committee Chair

University of California, Los Angeles

2013

Acknowledgements and Dedication

I would like to express my sincere gratitude to my advisor Professor Kendall N. Houk for his continuous support during both my undergraduate study and graduate research. I would like to thank all the professors in the organic division for introducing to me organic chemistry as well as for the motivation and support throughout my undergraduate years at UCLA. I am particularly grateful for the assistance and insightful comments given by Ashay Patel and Dr. Colin Lam on this project.

This thesis is dedicated to my beloved parents for their endless encouragement and support.

Table of Contents

Abstract	<i>ii</i>
Acknowledgements and Dedication	<i>iv</i>
List of Figures	<i>vii</i>
List of Tables	<i>vii</i>
List of Schemes	<i>viii</i>

Origins of Reactivity and Selectivity of a Series of Proximity-Induced Transannular Diels-Alder Reactions

I. Introduction.....	1
II. Background	2
2.1 Transannular Diels-Alder Cycloaddition	2
2.1.1 The synthesis of macrocyclic trienes	2
2.1.2 The Pd(II)-catalyzed macrocyclization strategy	4
2.1.3 The remarkably facile TADA reaction	5
III. Methods.....	5
3.1 Density Functional Theory (DFT)	5
3.2 Basis Sets	7
3.3 Self-Consistent Reaction Field (SCRF) Methods for Solvation	8
3.4 Monte Carlo Conformational Sampling.....	9

3.5 Potential Energy Surface (PES) Scan	9
3.6 Intrinsic Reaction Coordinate (IRC) Calculation.....	10
IV. Results and Discussion	10
4.1 Origins of TADA Stereoselectivity.....	10
4.1.1 Stereoselectivity of TADA reactions – background	10
4.1.2 <i>Exo</i> -(TST) selectivity	11
4.1.3 Discussion of TADA stereoselectivity.....	19
4.2 The Origin of Reactivity in TADA Cycloadditions.....	19
4.2.1 Choice of Model Reactions.....	20
4.2.2 Computed energy profile for all model reactions	21
4.2.3 Distortion/interaction model – background	23
4.2.4 Distortion/interaction energy analysis – modifications for TADA.....	27
4.2.5 Conformational entropy analysis on intramolecular Diels-Alder reaction	30
4.2.6 Discussion of TADA reactivities	32
4.3 Conclusions.....	32
V. References	33

List of Figures

1	<i>Endo</i> -transition state geometries of triene 1b	13
2	<i>Exo</i> -transition state geometries of triene 1b	14
3	The cbc transition state structures of 3a and 3b	15
4	The cbc transition state structures of 3c and 3d	17
5	Distortion/interaction energy model applied to a Diels-Alder reaction	24

List of Tables

1	Macrocyclic trienes and the corresponding tricyclic TADA adducts	11
2	Computed stereoselectivities of four TADA model reactions	12
3	Distortion energies of TADA tether fragments	18
4	Bimolecular, intramolecular, and transannular Diels-Alder reactions 1a – 1h	21
5	Comparison of computed and experimental ΔG^\ddagger at experimental temperatures	22
6	Computed ΔH^\ddagger and ΔG^\ddagger of BMDA, IMDA, and TADA reactions	23
7	Proximity-induced IMDA and the distortion/interaction model	26
8	TADA and the distortion/interaction model	28
9	Comparison of computed apparent activation energies and activation enthalpies	29

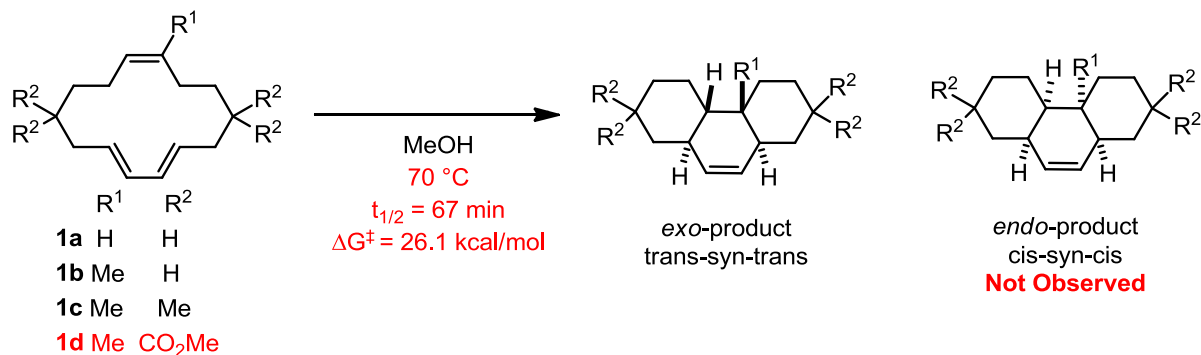
10	Computed ΔH^\ddagger and ΔG^\ddagger of BMDA, IMDA, and TADA reactions without S_{conf}	30
----	---	----

List of Schemes

1	Experimental results and computational scope of TADA reactions	1
2	Macrocyclization by an S_N2 reaction	3
3	Deslongchamp's Stille macrocyclization	3
4	TADA system using Pd(II)-catalysis developed by Merlic	4
5	Rate comparison between reactions 1h and 4a	25

I. Introduction

The Diels-Alder cycloaddition reaction has been widely employed in organic synthesis since its discovery in 1928.¹ In particular, the transannular Diels-Alder cycloaddition is effective in giving rise to tricyclic molecules with predictable stereochemistry at the ring junctions, which can serve as the structural backbone for a wide range of natural products.² For example, the TADA strategy has been applied in the total synthesis of (-)-oblongolide, momilactone A, (+)-maritamol, and in the preparation of the core skeletons of other useful compounds.³⁻⁶ Therefore, it is of great interest to organic chemists to develop the synthesis of macrocyclic trienes set up for a transannular Diels-Alder (TADA) reaction. Deslongchamps and coworkers were the first to report such method of macrocyclization in 1991, utilizing Pd(0) catalyst to prepare 10- to 14-membered rings.⁷ In 2012, Merlic et al developed a different method to more efficiently prepare cyclic targets in two steps from α,ω -diynes.⁸ Upon cyclization, the macrocyclic substrates underwent transannular Diels-Alder reaction stereoselectively under remarkably mild conditions. This thesis describes a computational study seeking to understand what factors are responsible for the reactivity and selectivity of these TADA reactions.



Scheme 1 Experimental results^a and computational scope of transannular Diels-Alder cycloaddition of macrocyclic trienes. ^a Experimental conditions are in red text.

II. Background

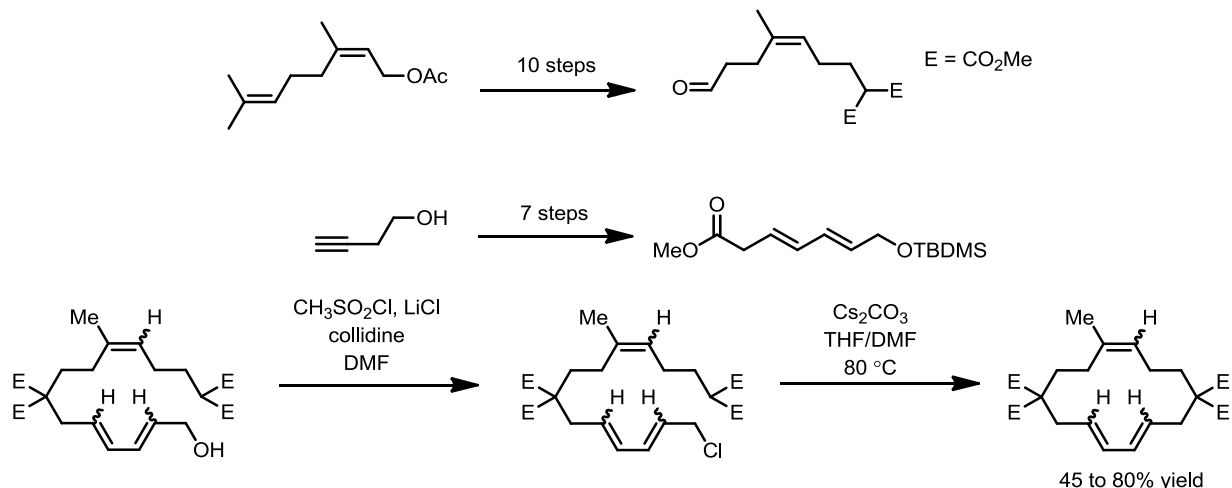
2.1 Transannular Diels-Alder Cycloaddition

The transannular Diels-Alder (TADA) cycloaddition reaction is one of the most efficient transformations in organic synthesis.⁹ TADA reactions exhibit higher reactivity compared to unimolecular Diels-Alder reactions.^{10,11} This is a result of both the entropic penalty prepaid from combining reactants into one complex and the conformational restrictions posed on the cyclic reactant.¹² TADA was first reported by Deslongchamps and coworkers as a new and efficient way to form the A.B.C.[x + 6 + y] type tricyclic compounds from macrocyclic molecules containing both the diene and dienophile motifs. TADA reactions allow for the formation of polycycles of well-defined stereochemistry. The most challenging step with the TADA strategy, or the bottleneck, as Deslongchamps phrased it, lies in the cyclization step to form the TADA substrate.^{13–15}

2.1.1 The synthesis of macrocyclic trienes

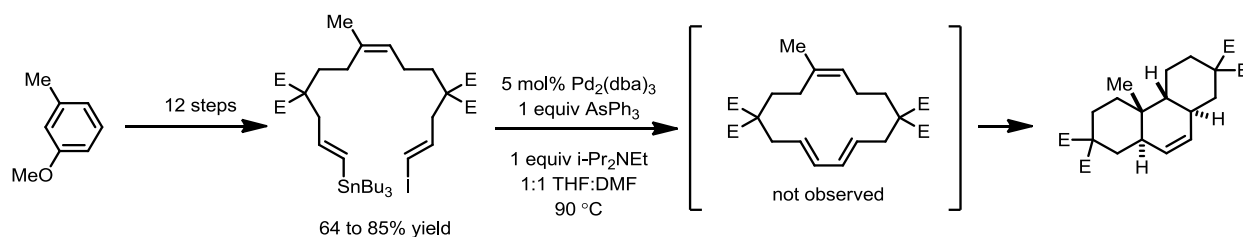
Deslongchamps' initial approach to prepare macrocyclic trienes relied upon malonate linkers to perform a cyclization via an S_N2 reaction.¹⁶ An example is shown in Scheme 2. The diene and dienophile fragments were constructed and connected together to form the acyclic triene. The allylic alcohol acyclic triene precursor was converted into their corresponding allylic chlorides. Macrocyclization was then carried out by deprotonation of the terminal malonic ester with cesium carbonate in tetrahydrofuran-dimethylformamide (1:1). It was followed by an S_N2 attack onto the allylic chloride for ring closure.¹⁷ This method provided a variety of macrocyclic trienes rapidly with different double bond configurations. However, it required linker motifs that needed to be elaborated subsequently, complicating the scheme for total syntheses. It also took

17 steps and involved numerous protection/deprotection procedures to synthesize the diene and dienophile fragments, which was not a step-economic approach to macrocyclization.



Scheme 2 Macrocyclization by an S_N2 reaction. The acyclic triene features malonic esters and allylic halide. The acyclic triene is assembled from diene and dienophile fragments synthesized independently.

A more efficient strategy for the synthesis of macrocyclic trienes involves forming the diene moiety during the macrocyclization step via Stille cross-coupling. This approach avoids the need for a connector that would have to be removed afterwards. Scheme 3 shows the Stille macrocyclization of the acyclic triene. With this approach, the malonic esters are no longer required for the ring closure.

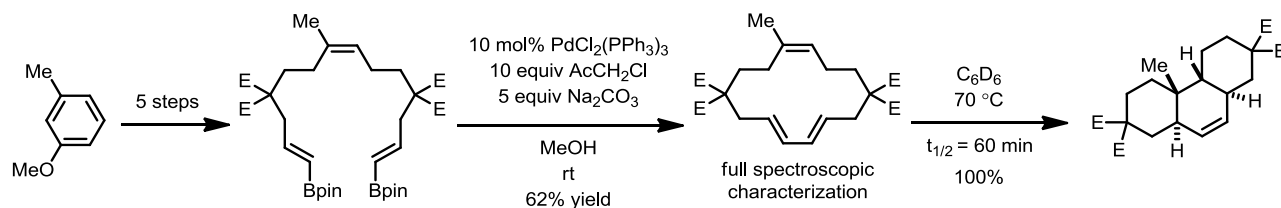


Scheme 3 Deslongchamp's Stille macrocyclization to prepare for TADA substrate.

2.1.2 The Pd(II)-catalyzed macrocyclization strategy

The Stille macrocyclization strategy developed by Deslongchamps in 2000 solved the key problem of preparing trienic macrocycles for TADA cycloadditions. However, there are limitations to the 13-step macrocyclization method. The use of vinyl halides can be toxic or carcinogenic, Pd(0) catalysts require an inert atmosphere, complex ligands are required to promote oxidative addition, and high temperature conditions can lead to product decomposition. Most importantly, the terminal groups need to be differentiated into electrophilic and nucleophilic components, leading to a more lengthy synthesis.

In 2012, Merlic and coworkers developed Pd(II)-catalyzed cross-coupling reactions to solve the inherent problems listed above in Pd(0)-catalyzed cross-couplings.¹⁸ In this approach, the cyclic trienes are prepared efficiently in 6 steps from commercially available materials.



Scheme 4 TADA system using Pd(II)-catalysis developed by Merlic.

Starting from 3-methylanisole, the α,ω -diyne was synthesized in five steps via Birch reduction, selective reductive ozonolysis, tosylation, and alkylation. Hydroboration with pinacolborane followed by the Pd(II)-catalyzed macrocyclization afforded the fully characterized triene in 62% yield.

2.1.3 The remarkably facile TADA reaction

The reaction of interest is shown in the last step of Scheme 4 above. The macrocyclic triene reacts very quickly with a half-life of 67 minutes at 70 °C with exclusive formation of the *exo*-product.

III. Methods

3.1 Density Functional Theory (DFT)

Density functional theory (DFT) is the computational method used to gain insight about the energetics and geometries of molecules in this project. The *ab initio* approach is grounded on the concept of wavefunction, which depends on the *x*, *y*, and *z* coordinates of each electron. Wavefunction theories give accurate energies and molecular properties, but the computational cost scales up rapidly as the size of the system increases. The Hohenberg-Kohn existence theorem proves the total energy of any system consisting of electrons is a unique functional of the electron density.¹⁹ DFT is a more direct and cost efficient way to obtain molecular energies, and it is the method used to give computational results presented in this thesis.

A benchmarking experiment testing three levels of theory was run: TPSS, B3LYP-D2, and M062X, all of which are Kohn-Sham density functional theory methods. These methods are known to accurately predict the thermodynamic and kinetic properties of main group organic reactions. The functional of Tao, Perdew, Staroverov, and Scuseria (TPSS) is a meta-generalized-gradient approximation (meta-GGA) functional.^{20, 21} The B3LYP hybrid functional is a combination of an exchange-energy functional established by Becke in 1993 and a correlation-energy functional by Lee, Yang, and Parr in 1988.^{22, 23} One weakness of B3LYP and

other hybrid functionals is they do not describe long-range electron correlation that is responsible for van der Waals dispersive forces.²⁴ This can be a major limitation of this approach for studying reactions involving changes in noncovalent interactions. The DFT problem for dispersion interactions has caught much attention in the recent years. Truhlar and Grimme independently developed parameterized methods for DFT to address this problem. Truhlar developed functionals that include short and medium-range dispersion corrections implicitly. Grimme developed explicit damped atom-pairwise dispersion corrections of the form $C_6 \cdot R^{-6}$, which is applied for a given set of atomic coordinates to provide the total energy as

$$E_{DFT-D} = E_{KS-DFT} + E_{\text{disp}} \quad (1)$$

where E_{KS-DFT} is the conventional Kohn-Sham energy obtained from DFT and E_{disp} is an empirical correction defined as

$$E_{\text{disp}} = -s_6 \sum_{i=1}^{N_{\text{at}}-1} \sum_{j=i+1}^{N_{\text{at}}} \frac{C_6^{ij}}{R_{ij}^6} f_{\text{dmp}}(R_{ij}). \quad (2)$$

N_{at} is the number of atoms in the system, C_6^{ij} is the dispersion coefficient for atom pair ij , s_6 is a global scaling factor specific to the DFT used, and R_{ij} is the interatomic distance.^{25, 26}

The dispersion correction term used to study our transannular Diels-Alder reaction is the B3LYP-D2 method of Grimme, which uses a simple pair-wise force field to describe the van der Waals interactions.

The M06-2X density functional is a variation of the so-called Minnesota family of functionals developed by Truhlar and coworkers and is suitable for main-group chemistry calculations.²⁷ This meta-hybrid GGA DFT functional depends on three variables: spin density (ρ_σ), reduced spin density x_σ , and spin kinetic energy density τ_σ . It is parameterized to account

for dispersion forces, improving one of the deficiencies of other DFT methods. According to a recent paper on transannular Diels-Alder reactivities, compared to coupled-cluster CCSD(T) calculations, which is a higher level of theory that requires huge computational resources, M06-2X calculations give more similar relative energies than those with B3LYP. All quantum mechanical calculations were performed using Gaussian 09.²⁸ All geometry optimizations and frequency calculations involved M06-2X/6-31+G** with a pruned integration grid consisting 99 radial and 590 angular points. The use of such a fine grid enhances calculation accuracy at minimal additional cost.

3.2 Basis Sets

Choosing the appropriate basis set is as important as selecting the appropriate level of theory for calculations on a particular molecular system. A basis set is a set of linearly combined mathematical functions used to describe atomic orbitals. Slater orbital (STO) functions are good approximations to atomic wavefunctions, but the use of Slater orbitals is impractical for large molecules since excessive computer time is required for integral evaluation. In general, a linear combination of Gaussian-type orbital (GTO) functions is used to approximate STO.²⁹ For geometry optimizations and frequency calculations of structures in this project, the split-valence double- ζ 6-31+G(d,p) basis set was used. The triple- ζ 6-311+G(d,p) basis set was used for single-point energy calculations.

It is well-known that the use of small basis sets in the calculation of interaction energies leads to an overestimation in the stability of the interacting complex relative to the separated reactants. The energies of molecules involved in an interacting complex can be too low because reactants share some basis functions. This “borrowing” of basis functions from the neighboring

molecules is termed basis set superposition error (BSSE). It effectively increases the overall basis set for each molecule, and thus gives lower energy values than the actual ones. BSSE is also observed in intramolecular systems, where one part of the molecule can use the basis functions from another part of the molecule. This problem is alleviated with larger basis sets.

The ‘+’ sign in the designation of the basis set denotes an extra set of Gaussian functions termed diffuse functions that more accurately represent the tail portion of the atomic orbitals. The addition of diffuse functions also better models GTOs to resemble STOs.^{30,31} They are usually used for systems that contain anionic species, or in our case, oxygen atoms with lone pairs.

The ‘d’ and ‘p’ in parenthesis in the end of the basis set are polarization functions. These basis functions are higher angular momentum orbitals. For example, the ‘d’ adds a d-type basis function to first row elements such as carbon and oxygen, and the ‘p’ adds a p-type basis function to the hydrogen atom, which has only an occupied s-type orbital. Polarization functions improve the flexibility of the basis set by giving a better representation of electron density in the bonding regions.

3.3 Self-Consistent Reaction Field (SCRF) Methods for Solvation

The Polarizable Continuum Model (PCM) was used to compute solvation free energies by creating a solute cavity via a set of overlapping spheres.^{32,33} This was done by placing the reactant, transition state, or product structures in a cavity within the solvent reaction field and calculating their energies with density functionals. Methanol was the solvent used.

3.4 Monte Carlo Conformational Sampling

The global minimum conformations for all ground state structures discussed in this thesis were located using conformational sampling. Reactant conformations of (*E*)-deca-1,3,9-triene were also generated to determine the conformational entropy of an intramolecular Diels-Alder reaction. Monte Carlo Multiple Minimum (MCMM) conformational searches were carried out using the MMFF force field in MacroModel.³⁴ New conformations were generated by randomly modifying the torsional angles for rotatable bonds in the input structure. The output conformers minimizing energies of the new conformers were minimized with the specified force field. 1000 optimization steps were used for each rotatable bond in the global search. Redundant conformer elimination is performed to remove high energy conformations. Force-field minimized structures were then optimized quantum mechanically with several DFT methods as discussed above.

3.5 Potential Energy Surface (PES) Scan

A PES scan can be used to efficiently describe the topology of a given reaction energy surface and to provide an initial guess for transition state calculations.³⁵ There are two types of PES scans: rigid and relaxed. A rigid scan involves altering one or more geometric parameters while performing single point energy calculations at each step. A relaxed scan changes geometric coordinates incrementally and performs a geometry optimization at each point, which is more costly but useful when the geometry of the rest of the molecule changes as bond formation/breaking takes place.³⁶ Transition states are verified by having one and only one imaginary frequency corresponding to the reaction coordinate.³⁷ Relaxed scans were performed for all transition states. Transition state geometries were located by performing relaxed PES scans followed by geometry optimizations of the structures located in the appropriate saddle-

point region of the PES. Using the two transition states found for the first model reaction as the starting guess geometries, the substituents on the ring were changed accordingly to locate the transition states of the remaining model reactions. Normal-mode analysis confirmed all transition states as first-order saddle points and all products and reactants as minima.

3.6 Intrinsic Reaction Coordinate (IRC) Calculation

An intrinsic reaction coordinate is a minimum-energy reaction path on a potential energy surface in mass-weighted coordinates.³⁸ Starting from a transition state geometry, an IRC calculation can trace a reaction path by integrating the intrinsic reaction coordinate following both the forward and backward directions.^{39,40} Initial force constants of the transition state are required for IRC calculations. IRC calculations were carried out to verify the genuine nature of the calculated transition state connecting adequate minima.

IV. Results and Discussion

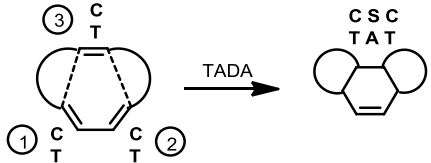
4.1 Origins of TADA Stereoselectivity

4.1.1 Stereoselectivity of TADA reactions – background

The TADA strategy generates a tricycle bearing four new stereogenic centers in one step, which means the tricycle can exist in eight racemic diastereomeric configurations. As studied both experimentally and computationally by Deslongchamps, the stereochemical outcome of TADA reactions can be predicted based on the reactant geometries of each double bond in the macrocyclic triene, and this can be employed in designing syntheses of natural products. Deslongchamps' quantum mechanical calculations of transition state geometries were carried out

at the RHF/3-21G level of theory.⁴¹ As shown in Table 1, macrocycles with *cis-cis* dienes do not undergo Diels-Alder reaction because the *s-cis* conformation is energetically costly, and the transition state geometry is highly strained. The *cis-trans* and *trans-cis* dienes readily adopt the *s-cis* conformation and undergo the reaction with *cis* or *trans* dienophile to form a single possible adduct. The *trans-trans* dienes, on the contrary, can form two adducts due to the higher flexibility of the ring. In these cases, substituents on the macrocyclic ring can influence the conformation of the transition state and the stereochemistry of the final adduct.

Table 1 Macrocyclic trienes and their corresponding tricyclic TADA adducts.⁴¹

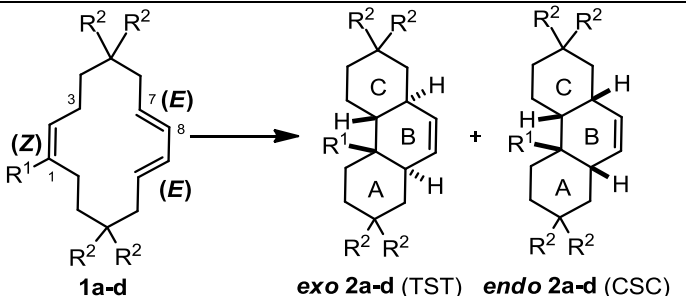
			
Macrocyclic triene		TADA product	
diene ① ②	dienophile ③	Computational	Experimental
CC (<i>cis-cis</i>)	C	CSC	no reaction
	T	no reaction	
CT (<i>cis-trans</i>)	C	CST (<i>cis-syn-trans</i>)	
	T	CAC (<i>cis-anti-cis</i>)	
TC	C	TSC	
	T	CAC	
TT	C	TST and/or CSC	
	T	TAC and/or CAT	

4.1.2 *Exo*-(TST) selectivity

According to Table 1, a *trans-trans-cis* (TTC) macrocyclic reactant would lead to two possible adducts, namely the *cis-syn-cis* (CSC) and *trans-syn-trans* (TST) products. Interestingly, the TADA reaction with macrocyclic triene **1d** carried out by Merlic and coworkers in Scheme 1 was observed to be exclusively *exo*-selective. That is, only the *trans-syn-trans* product was formed. To study this *exo*-selectivity of our TADA reaction, a series of model systems tabulated

in Table 2 was constructed to allow for careful examination of the effect of each substituent on the macrocyclic ring. These stereoselectivities were studied by Deslongchamps at the RHF/3-21G theory level. Higher levels of theory were used here to better explain the observed stereoselectivities.

Table 2 Computed stereoselectivities of four TADA model reactions computed at three levels of theory.

						
				$\Delta\Delta G^\ddagger^a$		
triene	entry	R ¹	R ²	TPSS	B3LYP-D2 ^b	M06-2X ^c
1a	1	H	H	-0.2	-0.6	-0.6
1b	2	Me	H	-0.2	-0.5	-1.0
1c	3	Me	Me	-3.6	-3.9	-4.4
1d	4	Me	CO ₂ Me	-1.4	-2.0	-2.1

^a $\Delta\Delta G^\ddagger = \Delta G^\ddagger(exo) - \Delta G^\ddagger(endo)$ in kcal/mol.

^b B3LYP-D2/6-311+G(d,p)//B3LYP-D2/6-31+G(d,p)

^c M06-2X/6-311+G(d,p)//M06-2X/6-31+G(d,p)

The four TADA model reactions with macrocyclic trienes **1a – d** shown in Table 2 are in the *trans-trans-cis* (*E,E,Z*) geometry, which allows flipping of both the diene and the dienophile. Consequently, two tricyclic products are predicted to form via the *endo*- or *exo*- transition states. The *endo*-transition states always lead to *cis-syn-cis* (CSC) tricycles, while the *exo*-transition states lead to *trans-syn-trans* (TST). Hence the terms *endo*- and *exo*- are used interchangeably with CSC and TST, respectively. Four geometries are possible for each transition state based on the conformations of the forming six-membered rings. The forming B ring would always adopt

the boat conformation as it is the required geometry for a Diels-Alder transition state.⁴² Both the A and C rings, however, could assume either the chair (c) or the twist-boat (b) geometries. Thus, the four possible geometries for the *endo*- and *exo*- transition states are bbb, bbc, cbb, and cbc.

Figures 1 and 2 show all eight transition geometries of the reaction of triene **1b**. For conformational simplicity, triene **1b** transition state geometries were studied instead of those of triene **1d**. The energies for each conformers shown were compared to the lowest energy cbc conformations in the *endo*- and *exo*-transition states.

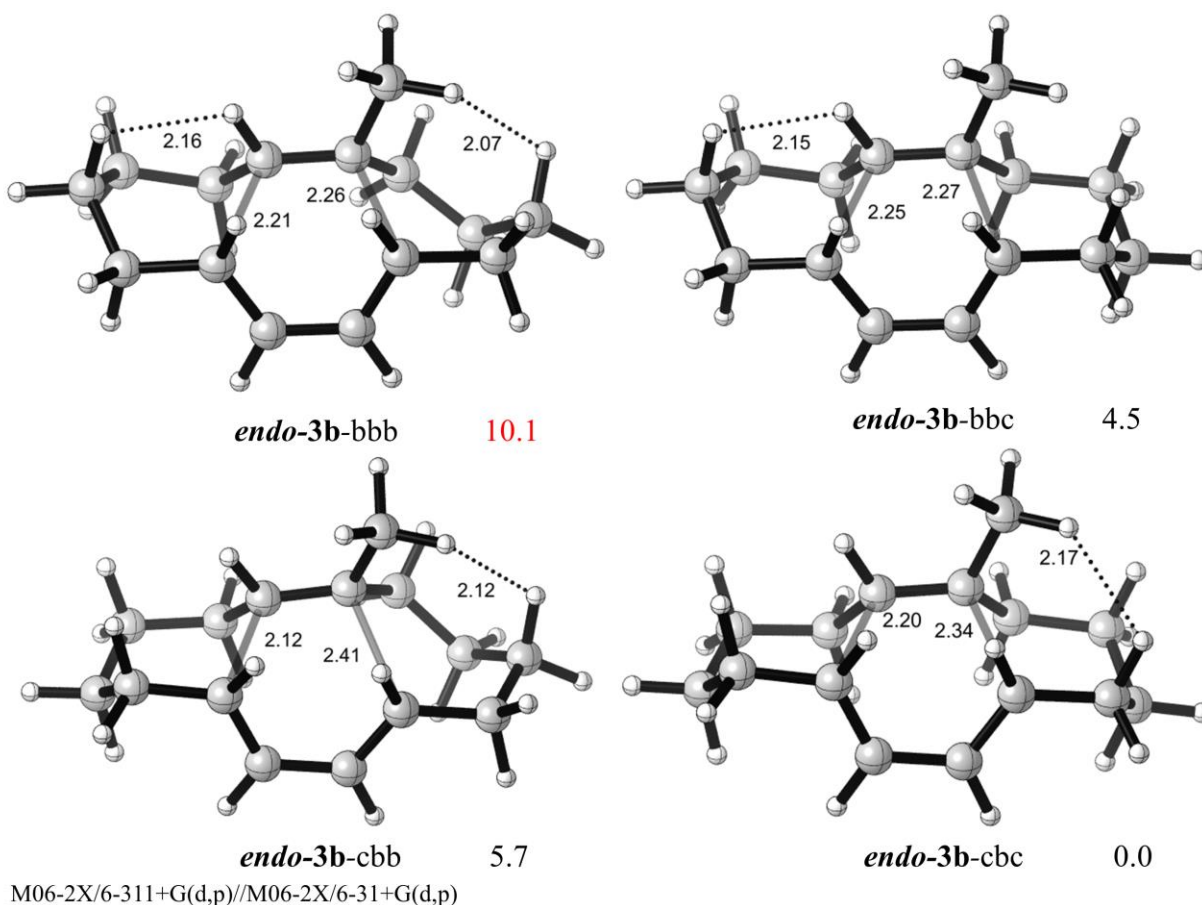


Figure 1 The bbb, bbc, cbb, and cbc *endo*-transition state geometries of the reaction of triene **1b**. $\Delta\Delta G^\ddagger$ values are shown in kcal/mol.

Frequency calculations indicated that the cbc geometries were favored over the other geometries for both the *endo*- and *exo*- transition states. Note the energy comparison is strictly

within each transition state, either *endo*- or *exo*-, and the two cbc conformations do not have the same energies. The bbc transition states were the next low energy conformers, which were 4 kcal/mol higher than cbc due to 1,4 flagpole interactions between the hydrogen in the R² position and diene hydrogen. The eclipsed bonds in the boat conformation also generated torsional strain that destabilized the geometry. This steric clash was even more severe in the cbb (best described as chair-boat-twist boat) geometry, in which the interaction was between the tether hydrogen and the methyl group on the diene, destabilizing the geometry by an addition 1.2 kcal/mol. The bbb geometries were not considered because they possessed steric clashes on both sides of the molecules and were at least 10 kcal/mol higher in energies than the cbc conformers.

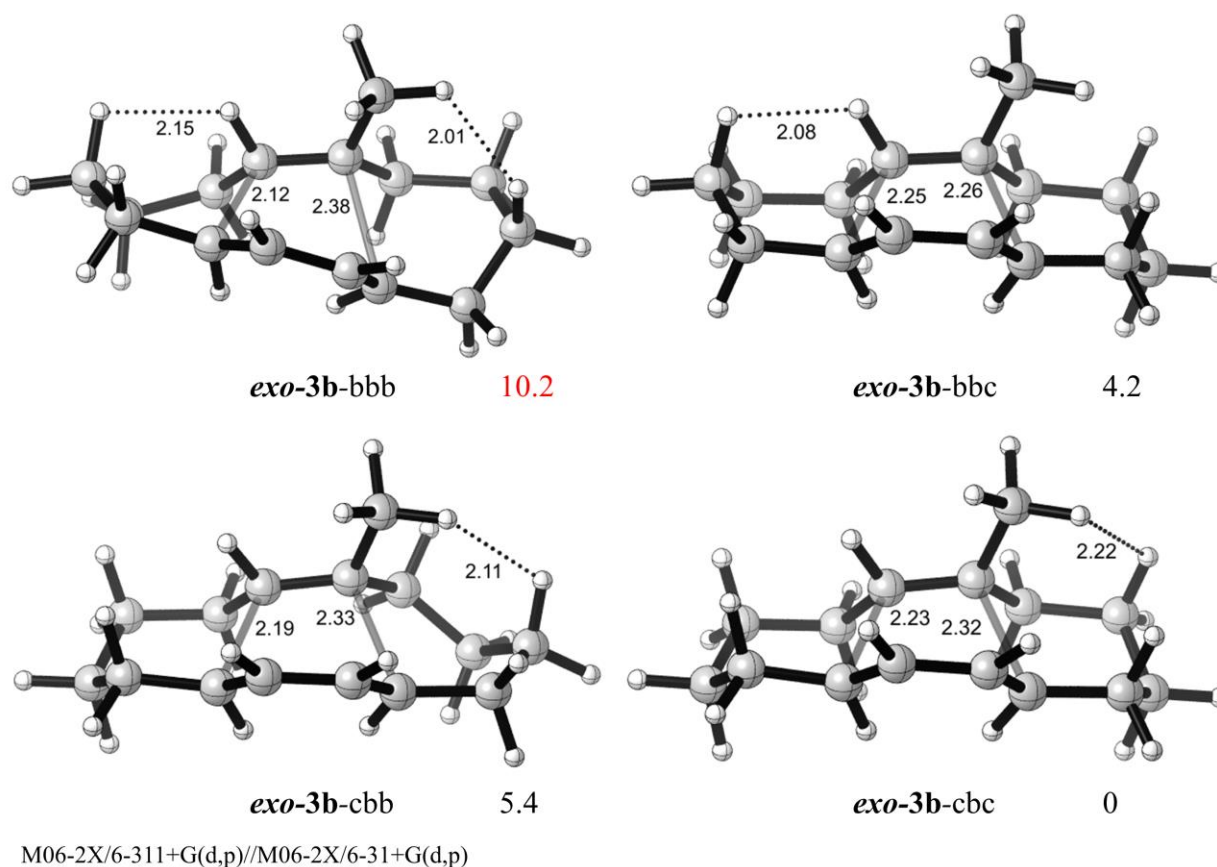


Figure 2 The bbb, bbc, cbb, and cbc *exo*-transition state geometries of the reaction of triene **1b**. $\Delta\Delta G^\ddagger$ values are shown in kcal/mol.

After determining the proper conformation for both the *endo*- and *exo*- transition states, the stereoselectivities of the reactions were investigated. The parent reaction with triene **1a** showed low selectivity. At the levels of theory investigated, the $\Delta\Delta G^\ddagger$ value was less than 1 kcal/mol favoring the *exo*-**3a** transition state (Table 2). Analysis of the two transition state geometries in Figure 2 A showed two 1,4 interactions between the diene hydrogens and the hydrogens on carbons 5 and 12 in the *endo*-transition state. The forming bond distances in both transition states were both 2.27 Å. There was a slight intrinsic preference for the *exo*-geometry, because the 1,4 interactions were not found.

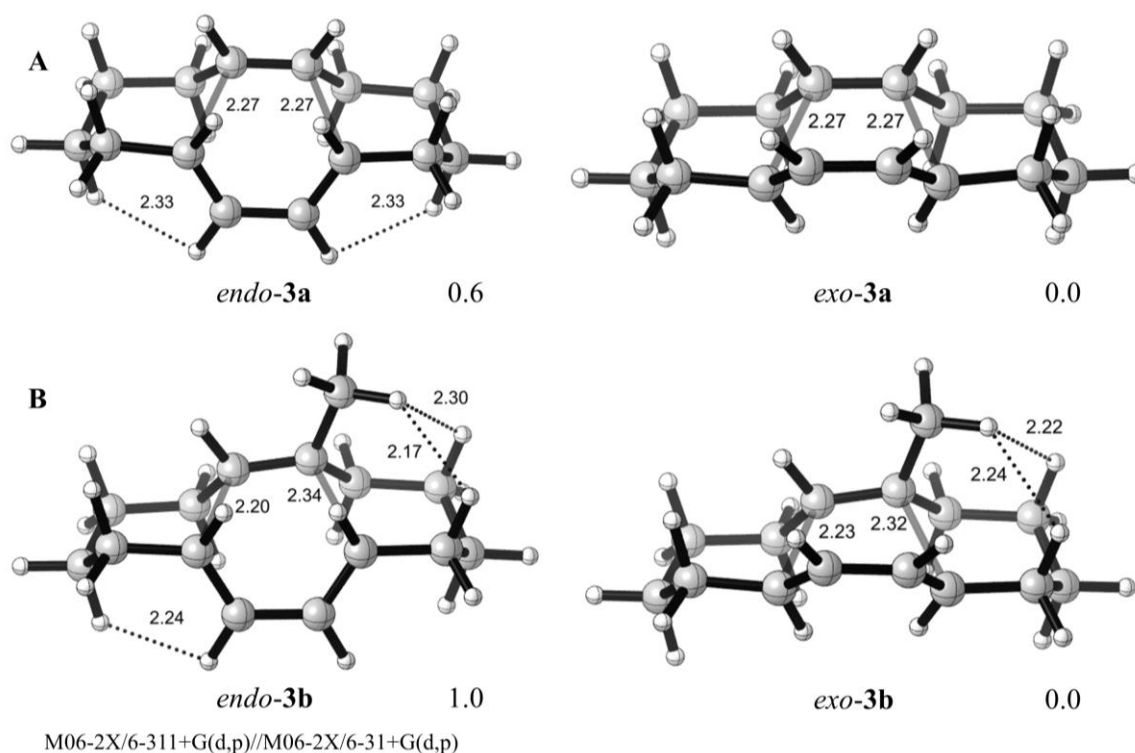


Figure 3 The cbc transition state structures **3a** and **3b** of TADA reactions of trienes **1a** and **1b**.

In the reaction with triene **1b**, the reaction proceeds through an asynchronous transition state. The forming bond lengths are 2.20 and 2.34 Å in the *endo*-**3b** transition state, and those in the *exo*-**3b** transition state are 2.23 and 2.32 Å. A slight 1,3-diaxial-like steric clash was observed

between the dienophile methyl hydrogen and the tether hydrogens in both the *endo*- and *exo*-transition states as shown in Figure 3 **B**. Since the methyl group at the R¹ position leads to steric clash in both transition states, it has no significant influence on the stereoselectivity of the reaction. This reaction has the same extent of *exo*-selectivity as the reaction with **1a**.

The stereoselectivity improves when R² is methyl instead of hydrogen (Table 2 entry 3). The presence of gem-dimethyl groups on the ring tethers increases the *exo*-selectivity of the reaction to 4.4 kcal/mol. A combination of fewer steric interactions and greater strain relief of the transition state are responsible for the *exo*-preference. Examining the *endo*-transition state structure shown in Figure 4 **C**, two severe syn-pentane-like interactions between the pseudoaxial gem-dimethyl hydrogen and the diene hydrogens on carbons 8 and 9 are observed. Calculations reveal that the two hydrogens are close in space with a separation of 2.06 Å (two van der Waals radii of H = 2.2 Å). In addition, the same gem-dimethyl groups have 1,3-diaxial interactions with the methylene hydrogens on carbons 3 and 13. These distances are measured to be 2.14 and 2.19 Å. On the other hand, the *exo*-transition state has four 1,3-diaxial-like interactions between the hydrogens on the diene and the gem-dimethyl groups. The extent of strain relief in the two pathways also plays a role in the selectivity of the reaction (Table 3). Strain relief of the tethers was determined by comparing the electronic energies of the tether fragments in their reactant and transition state geometries. The dotted portions of the trienes were removed, and the carbons were capped with hydrogen atoms at a distance of 1.09 Å. In the *exo*-pathway, a strain relief in the tethers of 6.7 kcal/mol is observed going from the reactive conformation to the transition state geometry. Only a 3.6 kcal/mol stabilization is seen in the *endo*-pathway. The lesser extent of strain relief is due to distortion of the tethers to avoid more severe steric clashes in the transition state geometry.

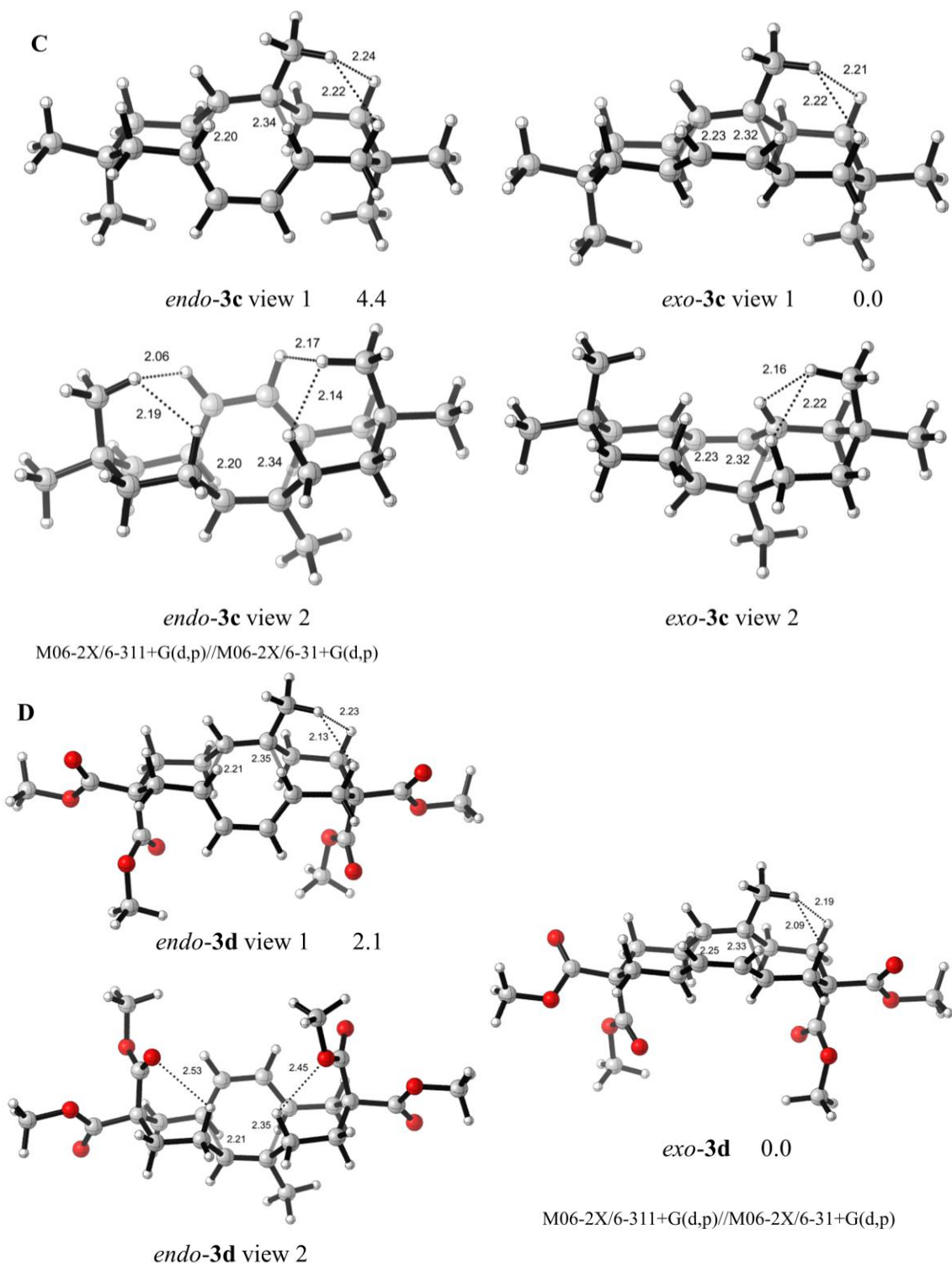
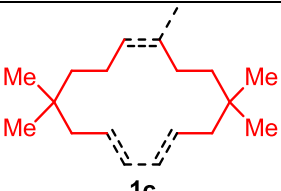
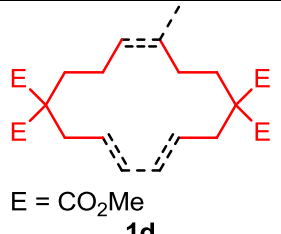


Figure 4 The cbc transition state structures **3c** and **3d** of TADA reactions of trienes **1c** and **d**. Two views of some geometries are shown. Bond lengths are in angstroms (Å).

After studying the three designed model substrates, we modeled the experimentally observed reaction with triene **1d**. In the computational system, the *exo*-**3d** transition state is more stable than the *endo*-**3d** transition state by 2.1 kcal/mol. The lower selectivity compared to the reaction with **1c** agrees with the observation that a methyl group has a larger A-value than an ester group. Consequently, fewer steric clashes were observed in the *endo*- and *exo*- transition states of this system (Figure 4 **D**). One interaction is between the pseudoaxial methyl ester carbonyl oxygen and the diene hydrogen in position 9; the other is between the pseudoaxial methyl carbonyl oxygen and the methylene hydrogen in position 3. Both C=O \cdots H distances were 2.50 Å, slightly shorter than the sum of the van der Waals radii of O and H (2.6 Å). No steric clash was found in the *exo*-transition state. The extent of strain relief in the *endo*-transition state was smaller by 2.7 kcal/mol. Distortion of the tethers was necessary to avoid steric clashes that would otherwise further destabilize the transition state geometry.

Table 3 A measure of the change in electronic energies of the tether fragments from reactant to transition state geometries is reported (kcal/mol) [B3LYP-D2/6-311+G(d,p)//B3LYP-D2/6-31+G(d,p)].

model	$\Delta E^{\ddagger}_{endo}$	$\Delta E^{\ddagger}_{exo}$
 <p>1c</p>	-6.7	-3.6
 <p>E = CO₂Me 1d</p>	-3.1	-0.5

4.1.3 Discussion of TADA stereoselectivity

The TADA reaction of *trans-trans-cis* 14-membered cyclic trienes could lead to two diastereomeric cycloadducts, but the *exo*-**2d** tricyclic diastereomer was the only product observed experimentally. Our computational data predicted the same outcome based on the relative energies of the two transition state structures. With no substituents on the ring, the TST-tricycle was inherently favored by less than 1 kcal/mol because the 1,5-interaction between the diene hydrogen and the tether hydrogen was found in the *endo*- but not in the *exo*-transition state. Addition of gem-dimethyl or gem-diester groups increased the *exo*-selectivity by introducing more pronounced 1,5-interactions and higher ring strain in the *endo*-transition state geometries. For the reaction with **1d**, the *exo*-pathway was favored by 2.1 kcal/mol, translating to a theoretical ratio of 88:12 *exo:endo* products, which was in good agreement with the experimental observation.

4.2 The Origin of Reactivity in TADA Cycloadditions

The prototype bimolecular Diels-Alder reaction between butadiene and ethylene to form cyclohexene requires thermal activation at 487 – 648 °C in gas-phase and has a range of activation free energies of 59.0 to 66.4 kcal/mol.^{43,44} The estimated activation free energy at 70 °C calculated using the Eyring equation is 39.9 kcal/mol. In comparison, the transannular version of Diels-Alder reaction carried out by Merlic and coworkers is observed to be remarkably facile. At 70 °C in methanol, the reaction proceeds with a half-life of 67 minutes, which translates into an activation free energy of 26.1 kcal/mol. The dramatic decrease in activation barrier without electronically activating groups has prompted us to investigate computationally the origin of the

reactivity of the TADA cycloaddition and come up with an explanation of the large activation free energy difference of almost 14 kcal/mol.

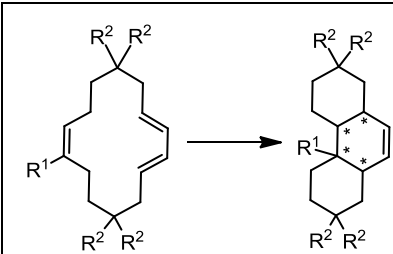
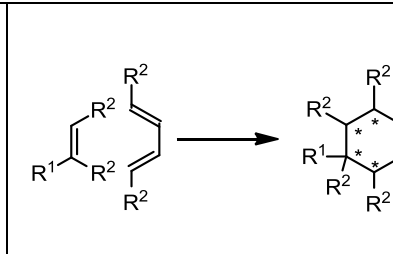
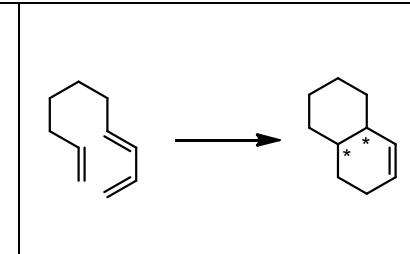
4.2.1 Choice of Model Reactions

To analyze the reactivities of the different versions of Diels-Alder cycloadditions, namely the bimolecular, intramolecular, and transannular reactions, we computed the reactant and transition state energies of a series of model reactions **1a** – **1d** shown in Table 2. The lowest energy s-cis conformation of the gem-diesters were located using dimethyl 2,2-dimethylmalonate as a model. The gem-diester fragments with the optimized conformation were installed onto the reactant **1d** and transition state **3d**. This procedure ensured that the energy difference between any species within the model was not due to difference in the geometries of the ester groups.

For the bimolecular Diels-Alder (BMDA) reaction, three model reactions were designed (Table 4). Reaction of **1e** was the cycloaddition of buta-1,3-diene and ethene. One methyl group was added onto ethylene in model 2 (**1f**) so as to mimic **1b** of TADA. In model 3 (**1g**), one methyl group was added to each terminus of both the diene and dienophile. This is to more accurately model the effect of the two tethers connecting the diene and dienophile moieties on TADA. This becomes important in section 4.2.4, where distortion/interaction energy analysis is performed on fragments of the macrocycles.

In addition to comparing the energetics between the bimolecular and transannular Diels-Alder reactions, we are also interested in comparing the reactivities of the intramolecular Diels-Alder (IMDA) and TADA, both of which are unimolecular reactions, to study the translational entropy of Diels-Alder cycloadditions. Our model for the IMDA reaction is (*E*)-deca-1,3,9-triene **1h**.

Table 4 BMDA, TADA, and IMDA model reactions **1a** – **1h**.

				
TADA (1a-d)		BMDA (1e-g)		IMDA (1h)
R ¹	R ²	R ¹	R ²	
H	H	H	H	
Me	H	Me	H	
Me	Me	Me	Me	
Me	CO ₂ Me	/	/	

4.2.2 Computed energy profile for all model reactions

A benchmarking of three density functional theory (DFT) methods showed that the M06-2X level of theory gave the most accurate energies that were within 2 kcal/mol of the experimental values. The TPSS method underestimated the energies up to 16 kcal/mol. B3LYP-D2 calculations gave more accurate results, but the computational values were still lower than the experimental values by approximately 6 kcal/mol. The series of TADA reactions was also modeled in the experimental solvent methanol using CPCM, and the results of which did not vary significantly from gas-phase calculations.

To assess the accuracy of the computational method chosen above, the activation free energies of BMDA, IMDA, and TADA cycloadditions were computed at their corresponding reaction temperature experimentally used. Results shown in Table 5 suggest the M06-2X level of theory gave the closest agreement to the experimentally measured values. To allow for direct comparison of kinetics among different reactions, all computations from this point on were performed at 25 °C in the gas-phase.

Table 5 Comparison of computed and experimental ΔG^\ddagger (kcal/mol) of BMDA, IMDA, and TADA reactions at experimental temperatures [M06-2X/6-311+G(d,p)/M06-2X/6-31+G(d,p)].

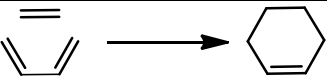
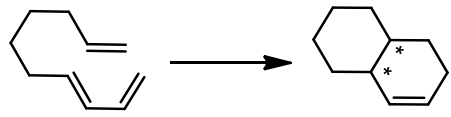
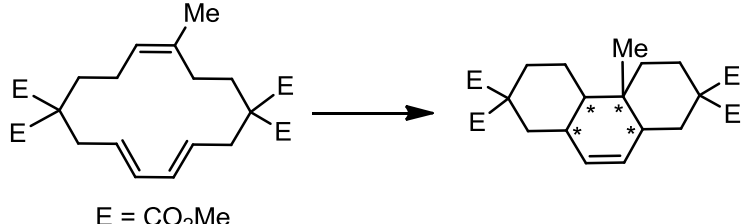
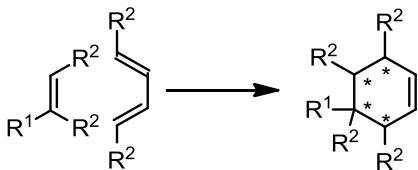
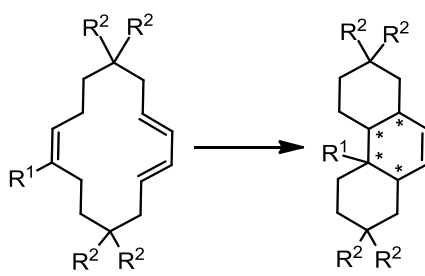
reaction	rxn temp.	$\Delta G^\ddagger_{\text{exp}}$	$\Delta G^\ddagger_{\text{calc}}$
	487 °C	59.0	54.1
	250 °C	34.5	30.6
 E = CO ₂ Me	70 °C	26.1	27.9

Table 6 shows the computed activation enthalpies and activation free energies of TADA reactions **1a** – **1d** and consequently BMDA reactions **1e** – **1g**. For the TADA series, the ΔH^\ddagger values remain relatively constant while the ΔG^\ddagger values increase down the column. The BMDA reaction series show an increase in both ΔH^\ddagger and ΔG^\ddagger as methyl groups are added to **1e**. Here, we compare the energies between the TADA reaction of **1d** and the BMDA reaction of **1g** as the methyl-substituted reactants of BMDA best mimic the effects of the tethers in the TADA system. Although the ΔG^\ddagger of TADA **1d** is 12 kcal/mol lower than that of the substituted BMDA **1g**, the ΔH^\ddagger for TADA is 1.7 kcal/mol higher. This indicates that the reactivity difference between BMDA and TADA cycloadditions is due solely to entropic differences. This result is puzzling because having the diene and dienophile moieties locked in a ring, the lowest energy conformation of a TADA reactant is expected to be more distorted from the untethered counterparts, and as a result, its geometry could become more transition state-like, decreasing the activation barrier. To further investigate the reactivities of the intermolecular, intramolecular,

and transannular Diels-Alder reactions, we apply the distortion/interaction model to these different hydrocarbon Diels-Alder reactions to gain more insight.

Table 6 Computed ΔH^\ddagger and ΔG^\ddagger (kcal/mol) of BMDA, TADA, and IMDA reactions at 25 °C in gas-phase [M06-2X/6-311+G(d,p)//M06-2X/6-31+G(d,p)].

						
			BMDA (1e-g)		TADA (1a-d)	
entry	R ¹	R ²	ΔH^\ddagger	ΔG^\ddagger	ΔH^\ddagger	ΔG^\ddagger
1	H	H	20.7	34.2	25.7	24.8
2	Me	H	21.6	35.5	25.8	28.7
3	Me	Me	23.4	39.9	26.1	28.7
4	Me	CO ₂ Me	/	/	25.1	27.9

4.2.3 Distortion/interaction model – background

The distortion/interaction model⁴⁵ has been used to study the reactivities and selectivities of a number of 1,3-dipolar^{46–48} and Diels-Alder cycloadditions.⁴⁹ In this model, the activation energy ΔE^\ddagger is decomposed into two parts, namely the distortion energy ΔE^\ddagger_d and the interaction energy ΔE^\ddagger_i : $\Delta E^\ddagger = \Delta E^\ddagger_d + \Delta E^\ddagger_i$. For a multi-molecular reaction, ΔE^\ddagger_d is defined as the total energy required to distort the geometry of each isolated reactant, butadiene and ethylene in the example of the reaction shown in Figure 5, into the geometry they acquire in the transition state without allowing interaction between reactants. ΔE^\ddagger_i is the interaction energy between the reacting components in the transition state, which is determined by subtracting the distortion energy from the activation energy. Analysis of unimolecular reactions using this model is

difficult because reacting groups are covalently tethered to one another. The example shown below will illustrate how the model has been modified to treat unimolecular systems.

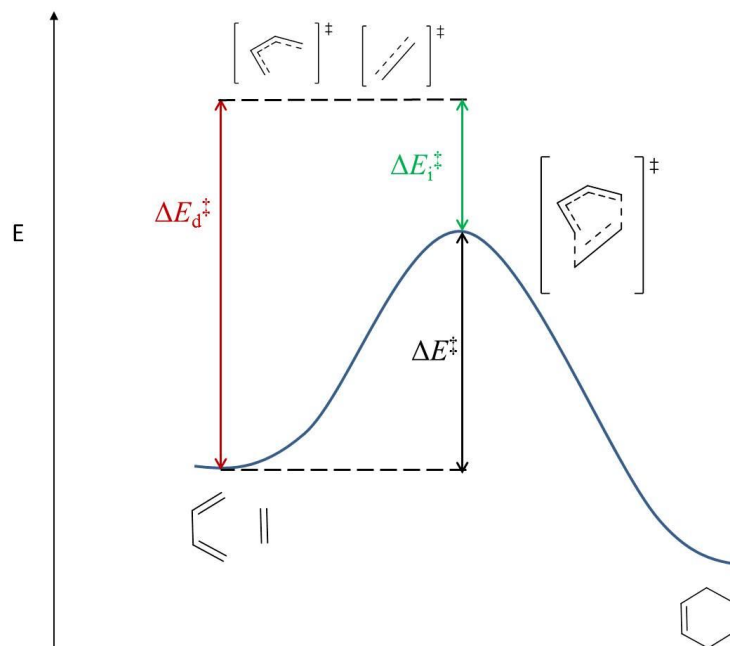
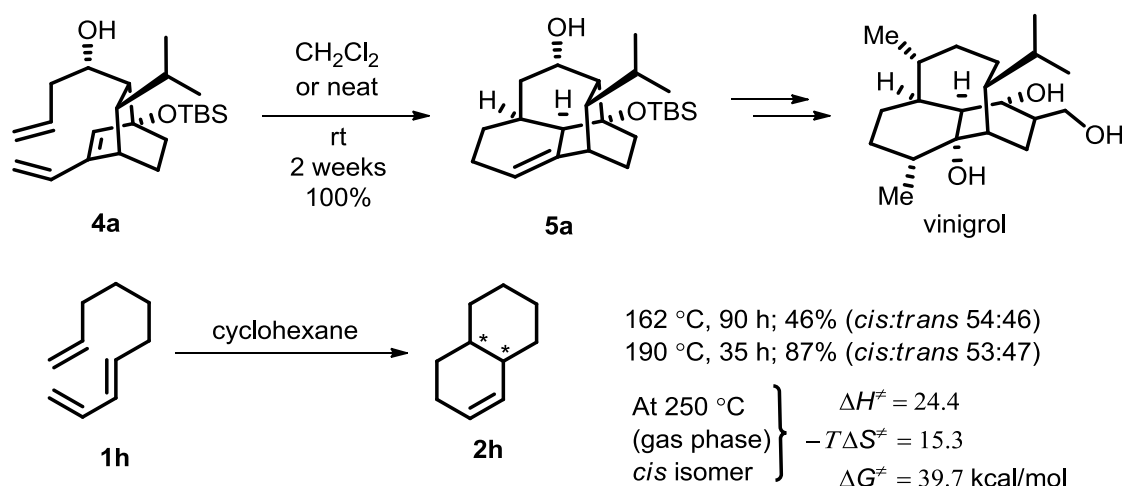


Figure 5 Schematic representation of the distortion/interaction energy model applied to the Diels-Alder reaction of buta-1,3-diene and ethene.

In the past, the distortion/interaction model has been modified to study the reactivity of a proximity-induced intramolecular Diels-Alder cycloaddition by Houk and coworkers.⁵⁰ Due to the unimolecular nature of the reaction, the distortion energy of the diene and dienophile cannot be assessed individually using the original model. To address this problem, an intramolecular version of the model was designed in which the single reactant was dissected into three moieties: diene, dienophile, and tether. The fragments were constructed by removing extraneous parts of the reactant and capping the carbons with hydrogen atoms at a distance of 1.09 Å.



Scheme 5 Rate comparison between reactions of **1h** and **4a**.

From Scheme 5, we see the proximity-induced intramolecular Diels-Alder reaction of **4a** occurs at room temperature, while reaction of **1h** requires elevated temperatures with significant lower yields. Table 7 shows the computed energies of a series of model reactions designed to study the reactivities of the proximity-induced IMDA. From the reaction of **1h** to **4a**, the ΔG^\ddagger is lowered by 4.3 kcal/mol. Breaking down the activation free energy term, we see that the ΔH^\ddagger is decreased by 3.3 kcal/mol, and $T\Delta S^\ddagger$ is decreased by 1 kcal/mol. This suggests the reaction rate of **4a** is increased by both favorable enthalpy and entropy compared to the reaction rate of **1h**.

To identify the structural features leading to the 3.3 kcal/mol rate acceleration, a distortion/interaction energy analysis was performed on these reactions. The right columns in Table 7 list the model fragments and their energies for each reaction. Addition of a methyl group on the dienophile in **5** slightly destabilizes the transition state by 1.5 kcal/mol. The distortion energies show that all three fragments in the reaction of **5** are more distorted than those in the reaction of **1h**. Transitioning to the reaction of **6** from **5**, there is a 3.8 kcal/mol rate increase. Placing the diene into the bicyclic ring system eliminates two degrees of freedom in bond rotations and reduces the diene distortion by 1.6 kcal/mol. The sum of distortion energies is 31.5

kcal/mol, which is 3 kcal/mol lower than that of the previous reaction ($E_d^\ddagger = 34.5$ kcal/mol). From **6** to **4a**, the total distortion energy is decreased by 6.6 ($\Delta E_d^\ddagger = 31.5 - 24.9$) kcal/mol. This is a result of distortion reduction in the diene and the tether. The bicyclic framework reduces the diene distortion by 3 kcal/mol. The tether is well stabilized by 4 kcal/mol down the column. This rate acceleration comes from strain introduced to the reactant geometry as well as hydrogen bond formation in the transition state geometry through the addition of functional groups to the bicycle.^{51,52}

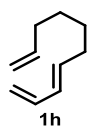
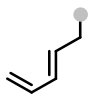
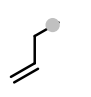
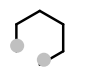
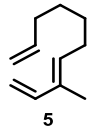
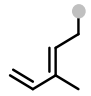
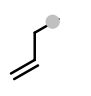
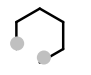
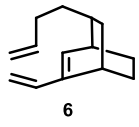
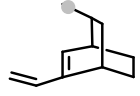
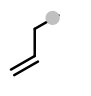
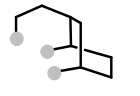
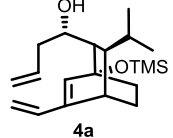
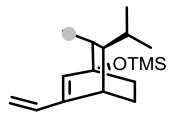
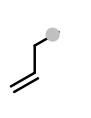
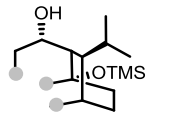
reactant	ΔG^\ddagger	ΔH^\ddagger	$T\Delta S^\ddagger$	model diene	E_{dist}^\ddagger (diene)	model dienophile	E_{dist}^\ddagger (dienophile)	model tether	E_{dist}^\ddagger (tether)
 1h	29.2	23.7	5.5		21.6		11.3		0.8
 5	30.7	24.9	5.8		21.7		11.8		1.0
 6	26.9	22.3	4.6		20.1		10.9		0.5
 4a	24.9	20.4	4.5		18.7		10.4		-3.2

Table 7 Analysis of factors contributing to acceleration of the intramolecular Diels-Alder reaction of **3**. Energies are reported at 25 °C in gas-phase (kcal/mol) [M06-2X/6-311+G(d,p)//B3LYP/6-31G(d)].⁴⁹

Through this example, one application of studying reactivity of an intramolecular Diels-Alder cycloaddition using the distortion/interaction model is described. As will be shown in the next section, we also find this method useful in understanding the reactivity of our transannular version of the (4 + 2) cycloaddition.

4.2.4 Distortion/interaction energy analysis – modifications for TADA

The example given in the previous section applied distortion/interaction energy analysis to explain the reactivity of the proximity-induced intramolecular Diels-Alder reaction. The distortion/interaction model showed that the increased reactivity of the proximity induced IMDA compared to other IMDAs comes from the drastic reduction in distortion energy. In section 4.2.2, however, we observe a constant activation enthalpy from intermolecular to transannular Diels-Alder cycloaddition. To gain insight into the factors that contribute to the reactivity of TADA reaction, a similarly modified version of the distortion/interaction model was employed.

Since the diene and dienophile in TADA are parts of a single macrocyclic structure, in order to analyze the distortion and interaction terms of each component of the cycloaddition, it was necessary to dissect the molecule into fragments before computing the electronic energies. Table 8 shows the fragments created for our distortion/interaction energy analysis. The macrocyclic triene **1d** was cut into four fragments: diene, dienophile, tether 1, and tether 2. Each of the four carbon-carbon bonds broken was capped by carbon-hydrogen bonds at 1.09 Å. The distortion and interaction energies of the TADA reaction were compared to those of the bimolecular reactions of **1f** and **1g** and intramolecular Diels-Alder reaction of **1i**. All structures in the remaining models were first optimized and dissected in a way that the diene and dienophile moieties were always butadiene and propene. Creating fragments of the same number of atoms allows for a more direct comparison of energy differences.

Table 8 Distortion and interaction energies for each of the four model Diels-Alder addends. The apparent activation energy is defined as the energy difference between the interacting transition state diene and dienophile fragments and the corresponding separate reactant geometries (kcal/mol) [B3LYP-D2/6-311+G(d,p)//B3LYP-D2/6-31+G(d,p)].

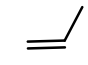
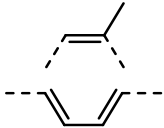
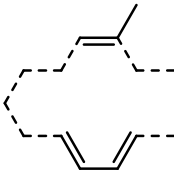
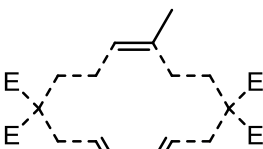
model	$\Delta E_{\text{d, diene}}^{\ddagger}$	$\Delta E_{\text{d, dienophile}}^{\ddagger}$	$\Delta E_{\text{d, total}}^{\ddagger}$	$\Delta E_{\text{i}}^{\ddagger}$	$E_{\text{a, (apparent)}}$
	16.9	10.7	27.6	-11.8	15.7
1f					
	17.0	14.6	31.6	-15.3	16.2
1g					
	15.7	13.7	29.4	-12.8	16.6
1i					
	13.0	12.2	25.2	-10.9	13.9
1d					

Table 8 shows the distortion and interaction energies of each model reaction diene and dienophile fragments. Optimized geometries are used along the reaction coordinate with **1f**. Therefore, the activation barrier is the actual E_{a} , which is the energy required to go from starting material geometries to the interacting transition state geometries. On the other hand, the E_{a} 's for reactions of **1g**, **1i**, and **1d** are the apparent activation energies, which are obtained by taking the energy difference between the transition state fragments and reactant fragments. Note the fragments are in their original geometries before which they are dissected. Comparing these values shows that there is no significant change in the overall activation energies among the three types of Diels-Alder cycloadditions. This is consistent with the observation that the three

reactions have similar ΔH^\ddagger values. We predicted the transannular reaction to have a smaller distortion energy due to conformational constraints within the macrocycle compared to the bimolecular and intramolecular reactions. This is indeed in agreement with the computed results, where the total distortion energy decreases by 6.4 kcal/mol from **1g** to **1d**. However, a corresponding weakening in interaction by 4 kcal/mol results in a small change in activation energies for the reactions.

A comparison of the apparent activation energies and the activation enthalpies suggest the tethers introduce disfavorable interactions in the transition state geometries that renders TADA slightly enthalpically disfavored compared to BMDA and IMDA. As shown in Table 9, while the apparent activation energy decreases down the column, the activation enthalpy increases. Furthermore, the difference between $E_{a, \text{apparent}}$ and $\Delta H^\ddagger_{\text{calc}}$ increases from 4.5 to 8.6 kcal/mol. This is an artifact from the removal of the tether(s) present in the structures of unimolecular reactions. Single point calculations of the complete structures of **1g** and **1d** followed by thermal corrections provided activation enthalpies that are much closer to the experimental values and suggest that this artifact goes away when the tethers are taken into account in the calculations.

Table 9 A comparison of the computed apparent activation energies and the activation enthalpies at 25 °C in the gas-phase (kcal/mol) [B3LYP-D2/6-311+G(d,p)//B3LYP-D2/6-31+G(d,p)].

model	$E_{a, \text{apparent}}$	$\Delta H^\ddagger_{\text{calc}}$
1f	15.7	20.2
1g	16.6	21.6
1d	13.9	22.5

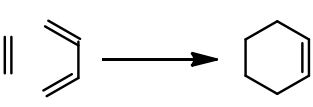
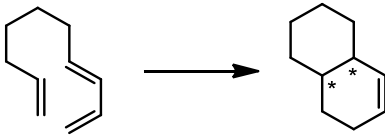
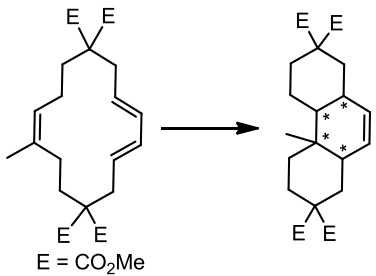
The above distortion/interaction energy analysis indicates that the remarkable increase in reactivity from BMDA to TADA cycloaddition is not due to favorable enthalpy.

4.2.5 Conformational entropy analysis on intramolecular Diels-Alder reaction

M06-2X calculations predict BMDA of **1e** to be 6.3 kcal/mol higher in activation free energy than TADA of **1d** at room temperature, which is in agreement with experimental results (Table 10). Comparing the activation free energies of IMDA of **1h** and TADA, however, shows that they only differ by 0.3 kcal/mol. This is not consistent with the difference in reactivity of the two reactions and with the harsher reaction conditions required for IMDA.⁵³ While reaction **1h** is performed at 250 °C in toluene, reaction **1d** proceeds with quantitative yields at 70 °C in methanol. Since both reactions are unimolecular, translational entropy of activation, which is accounted for in the activation free energy calculations, is expected to be similar. On the other hand, the activation conformational entropy of the more flexible system, which is not included in the calculations, may be responsible for the extra energy required for IMDA.

Table 10 Computed ΔH^\ddagger and ΔG^\ddagger of BMDA, IMDA, and TADA cycloadditions without S_{conf} at 25 °C in the gas-phase (kcal/mol) [M06-2X/6-311+G(d,p)//M06-2X/6-31+G(d,p)].

^a. experimental values estimated at 25 °C

					
BMDA (1e)		IMDA (1h)		TADA (1d)	
ΔH^\ddagger	ΔG^\ddagger	ΔH^\ddagger	ΔG^\ddagger	ΔH^\ddagger	ΔG^\ddagger
20.7	34.2 (37.8) ^a	23.3	27.6 (34.5) ^a	25.1	27.9 (26.1) ^a

The conformational entropy of activation is the entropy associated with the loss of conformational freedom from reactant to transition state. Previously, Priyakumar and coworkers have proposed that reactivity of transannular reactions increases as the probability that the

reactant is in the preferred conformation increases.⁵⁴ For TADA, there are few conformers other than the reactive conformer that contribute to the pool of reactant geometries. This is due to restricted rotation of many bonds in the macrocycle. Conversely, the acyclic substrates in non transannular unimolecular reactions are much more flexible because it has one tether fewer that connects the diene and dienophile moieties. All six single bonds can rotate freely and generates many more possible reactant conformers.

The activation conformational entropy (S_{conf}) was calculated using the following formula was used:

$$S_{\text{conf}} = -nR \sum_{i=1}^r x_i \ln x_i \quad (3)$$

where n is the number of moles, R is the gas constant, and x_i is the mole fraction of conformer i in the ensemble of r conformers. A Monte Carlo conformational search using the MMFF force field was performed to identify the low energy reactant conformers. The conformational search screened around all six rotatable C-C bonds, and isomers within 6.5 kcal/mol of the lowest energy conformer were counted at a calculation at 250 °C. The mole fraction of each conformer present was calculated using a Boltzmann distribution.

The activation conformation entropy was computed to be 4.9 e.u. The corrected activation free energy at 25 °C was 29.8 kcal/mol, and that at 250 °C was 37.0 kcal/mol, the latter of which was close to the experimental ΔG^\ddagger of 34.5 kcal/mol. The difference in conformational entropy in this case accounted for most of the reactivity improvement from IMDA to TADA cycloadditions.

4.2.6 Discussion of TADA reactivities

A series of transannular Diels-Alder cycloadditions was observed to be remarkably facile in comparison to the bimolecular and intramolecular versions previously studied experimentally. The distortion/interaction energy analysis suggests the rate acceleration of TADA **1d** compared to BMDA **1e** is not from favorable activation enthalpy; entropy is the major contributor to the rate acceleration from intermolecular to transannular Diels-Alder reactions. The difference in activation free energies between TADA **1d** and IMDA **1h** can be accounted for by the conformational entropy. The more flexible open-chain triene **1h** has more degrees of freedom and requires higher energy to achieve its reactive conformation for a Diels-Alder cycloaddition.

4.3 Conclusions

Computational study reported in this thesis aimed to explain the origins of stereoselectivity and reactivity of the TADA cycloaddition observed experimentally. Rules controlling the rate and outcome of this reaction were drawn out from both computational and experimental results.

1. This reaction shows excellent *exo*-preference due to the steric factors imposed in the trienic substrate that destabilizes the *endo*-transition state geometry. The *trans-syn-trans* (*exo*-) product without germinal substituents is inherently favored over the *cis-syn-cis* (*endo*-) product by less than 1 kcal/mol. This is mainly due to the 1,4 interactions in the *endo*-transition state that is absent in the *exo*-transition state.
2. For all transition states, the *cbc* macrocycle geometry is favored.

3. The increased reactivity of the reaction originated from the prepaid translational and conformational entropies not found in the bimolecular and intramolecular Diels-Alder reactions. Enthalpy does not play a role in the rate improvement of the TADA reaction.

These results allow synthetic chemists to employ transannular Diels-Alder reaction for macrocyclization towards total synthesis of complex molecules with a higher level of understanding of the stereoselectivity and reactivity of the reaction.

V. References

1. Diels, V. O.; Alder, K. *Liebigs Annalen* **1928**, 460, 98.
2. Marsault, E.; Toró, A.; Nowak, P.; Deslongchamps, P. *Tetrahedron* **2001**, 57, 4243.
3. Shing, T. K. *J. Chem. Soc., Chem. Commun.* **1986**, 49.
4. Germain, J.; Deslongchamps, P.; *Tetrahedron Lett.* **1999**, 40, 4051.
5. Toró, A.; Nowak, P.; Deslongchamps, P. *J. Am. Chem. Soc.* **2000**, 122, 4526.
6. Phoenix, S.; Reddy, M. S.; Deslongchamps, P. *J. Am. Chem. Soc.* **2008**, 130, 13989.
7. Deslongchamps, P. *Aldrichim. Acta* **1991**, 24, 43.
8. Iafe, R. G.; Kuo, J. L.; Hochstatter, D. G.; Saga, T.; Turner, J. W.; Merlic, C. A. *Org. Lett.* **2013**, 15, 582.
9. Deslongchamps, P. *Pure Appl. Chem.* **1992**, 64, 1831.
10. Xu, Y.-C.; Cantin, M.; Deslongchamps, P. *Can. J. Chem.* **1990**, 68, 2137.
11. For a review on IMDA reactions, see: Roush, W. R. In *Intramolecular Diels-Alder Reactions*; Paquette, L. A.; Ed.; Comprehensive organic synthesis; Pergamon: New York, 1991; pp. 513—550.
12. Roberge, J. Y.; Giguere, P.; Soucy, P.; Dory, Y. L.; Deslongchamps, P. *Can. J. Chem.* **1994**, 72, 1820.

13. Marsault, E.; Deslongchamps, P. *Org. Lett.* **2000**, *21*, 3317.
14. Roxburgh, C. J. *Tetrahedron* **1995**, *51*, 9767.
15. Fürstner, A. *Angew. Chem. Int. Ed. Engl.* **2000**, *39*, 3012.
16. Lamothe, S.; Ndibwami, A.; Deslongchamps, P. *Tetrahedron Lett.* **1988**, *29*, 1639.
17. Ndibwami, A.; Lamothe, S.; Soucy, P.; Goldstein, S.; Deslongchamps, P. *Can. J. Chem.* **1993**, *71*, 714.
18. Iafe, R. G.; Chan, D. G.; Kuo, J. L.; Boon, B. A.; Faizi, D. J.; Saga, T.; Turner, J. W.; Merlic, C. A. *Org. Lett.* **2012**, *14*, 4282.
19. Geerlings, P.; Proft, F. D.; Langenaeker, W. *Chem. Rev.* **2003**, *103*, 1793.
20. Tao, J. M.; Perdew, J. P.; Staroverov, V. N.; Scuseria, G. E. *Phys. Rev. Lett.* **2003**, *91*, 146401.
21. Kanai, Y.; Wang, X.; Selloni, A.; Car, R. *J. Chem. Phys.* **2006**, *125*, 234104.
22. Becke, A. *J. Chem. Phys.* **1993**, *98*, 5648.
23. Lee, C.; Yang, W.; Parr, R. G. *Phys. Rev.* **1988**, *37*, 785.
24. Gill, P. M. W.; Pople, J. A. *Chem. Phys. Lett.* **1992**, *197*, 499.
25. Grimme, S. *J. Comp. Chem.* **2006**, *27*, 1787.
26. Kruse, H.; Goerigk, L.; Grimme, S. *J. Org. Chem.* **2012**, *77*, 10824.
27. Zhao, Y.; Truhlar, D. G. *Theor. Chem. Acc.* **2007**, *120*, 215.
28. Gaussian 09, Revision C.01, M. J. Frisch, G. W. Trucks, H. B. Schlegel, G. E. Scuseria, M. A. Robb, J. R. Cheeseman, G. Scalmani, V. Barone, B. Mennucci, G. A. Petersson, H. Nakatsuji, M. Caricato, X. Li, H. P. Hratchian, A. F. Izmaylov, J. Bloino, G. Zheng, J. L. Sonnenberg, M. Hada, M. Ehara, K. Toyota, R. Fukuda, J. Hasegawa, M. Ishida, T. Nakajima, Y. Honda, O. Kitao, H. Nakai, T. Vreven, J. A. Montgomery, Jr., J. E. Peralta,

- F. Ogliaro, M. Bearpark, J. J. Heyd, E. Brothers, K. N. Kudin, V. N. Staroverov, T. Keith, R. Kobayashi, J. Normand, K. Raghavachari, A. Rendell, J. C. Burant, S. S. Iyengar, J. Tomasi, M. Cossi, N. Rega, J. M. Millam, M. Klene, J. E. Knox, J. B. Cross, V. Bakken, C. Adamo, J. Jaramillo, R. Gomperts, R. E. Stratmann, O. Yazyev, A. J. Austin, R. Cammi, C. Pomelli, J. W. Ochterski, R. L. Martin, K. Morokuma, V. G. Zakrzewski, G. A. Voth, P. Salvador, J. J. Dannenberg, S. Dapprich, A. D. Daniels, O. Farkas, J. B.
29. Goodman, J. M. *Chemical Applications of Molecular Modeling*. The Royal Society of Chemistry: Cambridge, 1998; p 216.
 30. Jensen, F. *J. Chem. Phys.* **2002**, *117*, 9234.
 31. Foresman, J. V. Ortiz, J. Cioslowski, and D. J. Fox, Gaussian, Inc., Wallingford CT, 2010.
 32. Tomasi, J.; Mennucci, B.; Cancès, E. *Theochem.* **1999**, *464*, 211.
 33. Scalmani, G.; Frisch, M. J. "Continuous surface charge polarizable continuum models of solvation. I. General formalism," *J. Chem. Phys.*, **132** (2010) 114110.
 34. MacroModel, version 9.6, Schrödinger, LLC, New York, NY, 2008.
 35. Mohamadi, F.; Richards, N. G. J.; Guida, W. C.; Liskamp, R.; Lipton, M.; Caufield, C.; Chang, G.; Hendrickson, T.; Still, W. C. *J. Comput. Chem.* **1990**, *11*, 440.
 36. Alder, R. W.; Harvey, J. N.; Lloyd-Jones, G. C.; Oliva, J. M. *J. Am. Chem. Soc.* **2010**, *132*, 8325.
 37. Foresman, J. B.; Frisch, M. *Exploring Chemistry with Electronic Structure Methods*, 2nd ed. (Gaussian, Inc., Pittsburgh, PA, 1996)
 38. Minkin, V. I. *Pure Appl. Chem.* **1991**, *71*, 1919.
 39. Zhixing, C. *Theor. Chim. Acta.*, **75** (1989) 481-84.

40. Fukui, K. *Acc. Chem. Res.* **1981**, *14*, 363.
41. Fortin, S.; Barriault, L.; Dory, Y. L.; Deslongchamps, P. *J. Am. Chem. Soc.* **2001**, *123*, 8210.
42. (a) Trost, B. M. *Science* **1991**, *254*, 1471. (b) Trost, B. M. *Angew. Chem. Int. Ed. Engl.* **1995**, *34*, 259.
43. Rowley, D.; Steiner, H. *Discuss. Faraday Soc.* **1951**, *27*, 5299.
44. Guner, V.; Khuong, K. S.; Leach, A. G.; Lee, P. S.; Bartberger, M. D.; Houk, K. N. *J. Phys. Chem. A* **2003**, *107*, 11445.
45. For reviews on the distortion/interaction model: te Velde, G.; Bickelhaupt, F. M.; Baerends, E. J.; Guerra, C. F.; van Gisbergen, S. J. A.; Snijders, J. G.; Ziegler, T. *J. Comput. Chem.* **2001**, *22*, 931.
46. Schoenebeck, F.; Ess, D. H.; Jones, G. O.; Houk, K. N. *J. Am. Chem. Soc.* **2009**, *131*, 8121.
47. Xu, L.; Doubleday, C. E.; Houk, K. N. *Angew. Chem. Int. Ed.* **2009**, *48*, 2746.
48. Ess, D. H.; Jones, G. O.; Houk, K. N. *Org. Lett.* **2008**, *10*, 1633.
49. Garc á, J. I.; Mart ínez-Merino, V.; Mayoral, J. A.; Salvatella, L. *J. Am. Chem. Soc.* **1998**, *120*, 2415.
50. Krenske, E. H.; Perry, E. W.; Jerome, S. V.; Maimone, T. J.; Baran, P. S.; Houk, K. N. *Org. Lett.* **2012**, *12*, 3016.
51. Paton, R. S.; Kim, S.; Ross, A. G.; Danishefsky, S. J.; Houk, K. N. *Angew. Chem. Int. Ed.* **2011**, *50*, 10366.

52. (a) Huisgen, R.; Möbius, L.; Müllwe, G.; Stangl, H.; Szeimies, G.; Vernon, J. M. *Chem. Ber.* **1965**, 98, 3992. (b) Huisgen, R.; Ooms, P. H. J.; Mingin, M.; Allinger, N. L. *J. Am. Chem. Soc.* **1980**, 102, 3951.
53. Diedrich, M. K.; Klärner, F. G.; Beno, B. R.; Houk, K. N.; Senderowitz, H.; Still, W. C. *J. Am. Chem. Soc.* **1997**, 119, 10255.
54. Prathyusha, V.; Ramakrishna, S.; Priyakumar, U. D. *J. Org. Chem.* **2012**, 77, 5371.